

Application of Support Vector Machine method in Hyperspectral mapping of Ophiolite mélanges-a Case study from eastern Iran

Hesam Moeinzadeh^{1*}, Hosein Fallahi², Ahmad Abbasnejad³, Saeed Goodarzi Mehr⁴, Bahram Bahrambeygi⁵

1- Assistant Professor, Department of Geology, Shahid Bahonar University of Kerman

2- MSc Geology, University of Birjand

3- Associate professor, Department of Geology, Shahid Bahonar University of Kerman

4- MSc Remote sensing, Department of Geography University of Tehran

5- PhD student, Department of Geology, Shahid Bahonar University of Kerman

* Corresponding Author: hesammoeinzadeh@yahoo.com

Received: 15 October 2013 / Accepted: 20 December 2013 / Published online: 25 December 2013

Abstract

The lithologies of regions, which located near the collision zone, are very different from other geology setting. Mapping in these areas needs extensive and exact studies and tools because of the variety of rocks, intensive tectonic uplift and complicated units. Hyperspectral sensor is one of the most advanced tools with hundreds of bands that each measures a very narrow range of wavelengths and continuous bands in visible and infrared spectrums, so it can identify various terrain despites with spectral similarities and complications. In present study, as the first survey of hyperspectral data efficiency for separating ophiolite melange units in Iran, we applied spectral - based method of support vector machine classification method on Hyperion image, in east of Iran. Based on various laboratory- field studies, the lithology of studied area can be separated into five general groups (ophiolite series, metamorphic units, Oligocene - Miocene to Quaternary volcanic units, limestone and flysh units). In this region for calculation of processing results accuracy rate, some scattered locations and points were sampled according to field surveys. These samples were analyzed in microscopic section and by electron microprobe. Points of Grand though selected based on these field-laboratory studies for compute results accuracy rate. According to results, the average overall accuracy for all lithology has reached 52% in total colored- mélanges of the studied area at the east of Iran. The user accuracy factor of SVM method is highest for the lithology with more spectral separability. These coefficients are acceptable ratios in separation of ophiolites as actual complicated units.

Keywords: Ophiolite, Hyper Spectral, Support Vector Machine (SVM), Iran.

1-Introduction

Ophiolite mélanges of Iran represent a part of an ophiolite belt extending from Pakistan via Iran to Turkey, Greece and some other countries in Europe (Ghazi *et al.*, 2004). The majority of these ophiolite outcrops contain a complete succession, although some outcrops are incomplete and occasionally are considered as colored mélanges as a result of tectonic

activities acting upon them. The ophiolites of Iran are grouped according to their age into Paleozoic (Weber-Diefenbach *et al.*, 1984) and Mesozoic (Arvin and Robinson; 1994) groups (Fig.1). The latter group is much more widespread and ophiolites of the studied area belong to this category. Hyperspectral mapping using spectroradiometry is a technology for attaining spectrometric data. Spectroradiometry is based on the interaction of surficial molecular

structure of a substance with electromagnetic waves impinging on it. Natural substances constituting the Earth's surface will absorb, reflect or scatter the electromagnetic waves according to their composition. It is possible to determine the spectrometric response of different substances. The resulting curves are used as indicators for identification of different substances and their composition (Clark *et al.*, 1993).

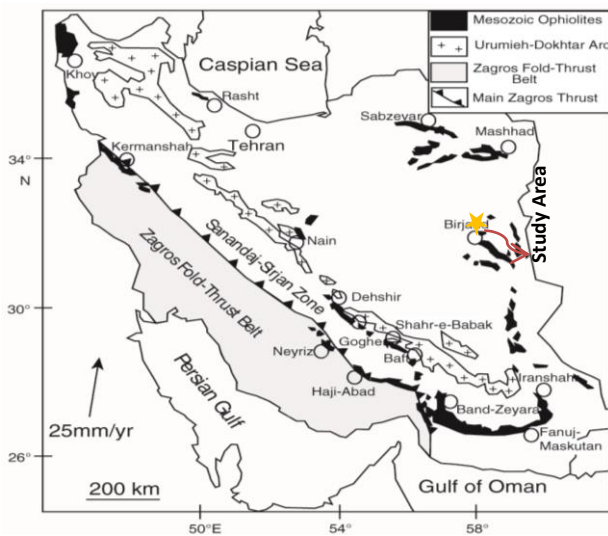


Figure 1) Distribution map of Mesozoic ophiolite belts of Iran (from Moghadam, *et al.* 2013).

Hyperspectral sensors are capable to image in numerous extremely narrow spectral bands. So, their spectral data can be used for determination of substances with very small differences in spectral patterns. Separation and mapping of ophiolite mélanges is usually challenging because they have very complex and cluttered units. Hence, hyperspectral mapping with field checking may facilitate their separation and mapping.

1.1–Hyperion sensor

Hyperion represents the first airborne hyperspectral sensor mounted on EO-1 platform. Hyperion images are taken in 242 narrow bands in wavelengths between 356 to 2577 nanometers with 10 nanometers spectral and 30 meters spatial resolution and each image includes a narrow band 7.7 km in width and 185 or 42km in length (Pearlman *et al.*, 2003).

These images are readily used in geological investigations (Kruse *et al.*, 2003; Xu *et al.*, 2014). Hyperspectral data may be used for studying spectral patterns of surficial materials. Hyperion sensor is a push broom system that covering a square area 7.7 km in length. Therefore, in these sensors, spectral data are recorded as three-dimensional cubic frames with totally 242 imaging bands.

1.2–Previous studies

Hyperion hyperspectral images have been used in agriculture, mineral exploration, separation of land units as well as other fields of geological sciences. For example, Kruse *et al.* (2003) have compared the capability of airborne hyperspectral data of Hyperion for spectral separation of land surface minerals. Hubbard *et al.* (2003) have compared mineral alteration mapping of visible to shortwave infrared Hyperion with ALI and ASTER images. In addition, using EO-1 Hyperion images, Kruse (2003) have prepared the hyperspectral map of coral reefs of Buck Island in central Atlantic Ocean. In addition, using EO-1 satellite data, Beiranvand Pour and Hashim (2011) have prepared the geological map of the southeastern part of the central Iranian Volcanic Belt. Some other relevant studies using hyperspectral data in geological investigations include Coops *et al.* (2002), Staenz *et al.*, (2002), Pearlman *et al.*, (2003), Felde *et al.*, (2003), Bindschodler and Choi (2003), Ramsey *et al.*, (2004), Khurshid *et al.*, (2006), Gersman *et al.*, (2008) and Leverington (2008). Geological investigations undertaken in the studied include Fotoohi Rad (1996, 2004 and 2009), Brocker *et al.*, (2005), Fotoohi Rad *et al.*, (2005) and Theunissen *et al.*, (2004). However, no remote sensing studies have taken place in this area up to now, and the present study is the first one to employ hyperspectral data for separation of ophiolite mélanges. About capable of spectral processing method that use for present study Kovacevic *et al.*, (2009) and Goodarzi Mehr *et al.*, (2012)

used support Vector Machine classification method for lithological mapping and gotten satisfactory results. Abedi *et al.*, (2011) used Support Vector Machine classification method for mineral mapping and exploration of porphyry-Cu deposits in Kerman province of Iran. Their results indicated the capability of SVM as a supervised learning algorithm tool for predictive mapping of mineral prospects. Also Goodarzi Mehr *et al.*, (2012) used support Vector Machine classification method for lithological mapping and compared potential of the SVM in different kernels with other methods. They concluded that SVM method has high capability in extraction and separation of lithological units.

1.3–Geological setting

The studied area lies in the structural zone of Sabzevar-Sistan, which formerly was described by Mc Call and Kidd (1981) and Tirrul *et al.*, (1983). In this zone, volcanic and plutonic rocks which are widespread include calc-alkaline volcanic rocks aging late Cretaceous-Paleocene. They are observed in the eastern and northeastern part of Sistan region and have been ascribed to subduction of an oceanic plate under the Afghan block (Tirrul *et al.*, 1983). Among the volcanic rocks aging Eocene- Pliocene, Eocene – Oligocene volcanics including Porphyry andesites, Pyroclastic and dacitic lavas are much more common. The oldest volcanic rocks, which have been named “Cheshmeh Ostad Group” (Tirrul *et al.*, 1983), are ophiolitic in character, although lack ultramafic and layered gabbro. Cheshmeh Ostad intrusive as well as calc-alkaline intrusives aging upper Eocene- lower Oligocene (including Zahidan granite) intruded into slightly metamorphosed marine detrital deposits of Neh complex (Camp and Griffis, 1982). The youngest volcanic activities in Sistan structural zone include Quaternary olivine basalts, which cover older units in the northern part of this zone. The studied ophiolite mélange is

intermingled with flyschs, which are partially metamorphosed, so that a major part of the ophiolites has been metamorphosed. There is a conspicuous metamorphosed zone in the eastern part of Eastern Iran ophiolites comprising green schists, epidote amphibolites, amphibolites, blue schists and eclogites. This metamorphic zone is very conspicuous (Fotoohi Rad, 1983). Such rocks play a key role in recognition of the tectonic environment and evolution of orogenic belts and commonly represent locations of oceanic crust seduction before collision of continental crusts (Bucher and Fry, 1994 and Gomes – Pugnair *et al.*, 2003). Oligocene – Miocene volcanic activities in eastern Iran include dacites, riodacites, andesitic dacites, porphyroidal quartz- diorites and andesitic basalts which commonly lie at the higher parts of the region.

2–Materials and Methods

2.1–Hyperion sensor

Preprocessing of data taken from Hyperion sensor include organization of bands in a form of processable digital data, calculation of central wavelength of spectrum and modification of this parameter in all bands, removing bad bands, erasing strip lines in image bands using cornels, and finally geometric and atmospheric corrections. In this studied, we used L1 data set of EO1-hyperion system that does not require some preparations such as stacking. In addition, since the studied area is located at the central part of satellite imaging belt and the MNF number of one, our data have not been too destroyed by streak or smile effect. In organization and filtration of image bands, 78 bands of the total 242 imaged bands wave wiped out due to unsuitable quality of data, So 155 bands were studied. Geometric correction was undertaken by images of Quickbird satellite mounted on the Global Positioning System (GPS) and via field studies. Atmospheric correction of Hyperion data performed using

Internal Average Relative Radiance (IARR) or relative average of reflectance as a suitable preprocessing for recovering spectral information on hyperspectral data in a semi-arid region.

2.2–Classification using SVM

The Support Vector Machines (SVM) method is a nonparametric and controlled statistical method and acts upon the premise that data set distribution types are unknown. The main character of this method is its high capability in using trained samples and attaining higher accuracy in comparison with other methods of classification (Montero *et al.*, 2005 and Mountrakis *et al.*, 2011). In reality, the support vector machine is a binary classification, which separates two classes by a linear boundary and relies on generalized linear classifiers (Bhambhu and Srisres Tava, 2009). SVM classifies the data by passing a plane (linear boundary) and by using all bands and employing an optimization algorithm. In this process, at first margin pixels were determined. In another words, a number of training points which are nearest to decision border were considered as support vectors. Although, increasing the dimensional of data leads to better results. In reality, if in spectral space the classes have interference, the data sets are transferred into a space with larger dimensionality so that their separation becomes possible. In this algorithm, the main purpose is to find the farthest distance between two classes which leads to more accurate classifications, while generalization error decreases (Zhang *et al.*, 2008). The main distinguishing component of SVM is the trend of this algorithm on a rule that is known as Structural Risk Minimization (SRM). In reality, the SVM minimizes the classification errors in unobserved data lacking. Statistical techniques such as maximum likelihood estimation usually assume that data

distribution is known a priori (Mountrakis *et al.*, 2011). The optimum border is used for determination of decision border at each completely-separated two classes. (Van Pik and Cher Voncnkis, 1991). The linear margin between the two classes is completed so that:

a) All samples belonging to +1class are located in one side of the border and all samples belonging to -1 class are located in the other side.

b) The decision border must be so selected that the distance of training samples between each couple of classes in orthogonal direction with respect to decision border becomes as maximized as possible (Keshavarz and Ghasemian Yazdi, 2007), i.e., in this method, firstly, the distance between the nearest training samples of the two adjacent classes in orthogonal directions are computed and subsequently by solving the optimization function, best margins are determined (Goodarzi Mehr *et al.*, 2012). Two parallel planes are defined in the two sides of decision border, so that the border plane contains the maximum equal distance with respect to these two plains. Generally increasing the distance between two parallel planes make higher accuracy of classification (Srivastava *et al.*, 2009). Actually, this algorithm seeks to find a hyperplane which can act so that while being compatible with training data, can separate the data set from each other (Mountrakis *et al.*, 2011).

An optimal hyperplane separates the classes with a decision surface that maximizes the margin between the classes (keshavarz and Ghasemian Yazdi, 2007). The optimized hyper plane separator term refers to a range which, by using training data, makes the number of incorrectly classified pixels minimized (Mountrakis *et al.*, 2011). There are several kernels for defining this border plane (Fig. 2).

Whenever the data cloud contains too much interference it is possible to use polynomial

kernel with different terms and gammas or use Radial Basis Function (RBF) kernels. The pertaining equations for these three kernels are the following:

LinearK $(x_i, x_j) = x_i^T x_j$

Polynomial $K(x_i, x_j) = (g x_i^T x_j + r)^d, g > 0$

RBF $K(x_i, x_j) = \exp(-g \|x_i - x_j\|^2), g > 0$

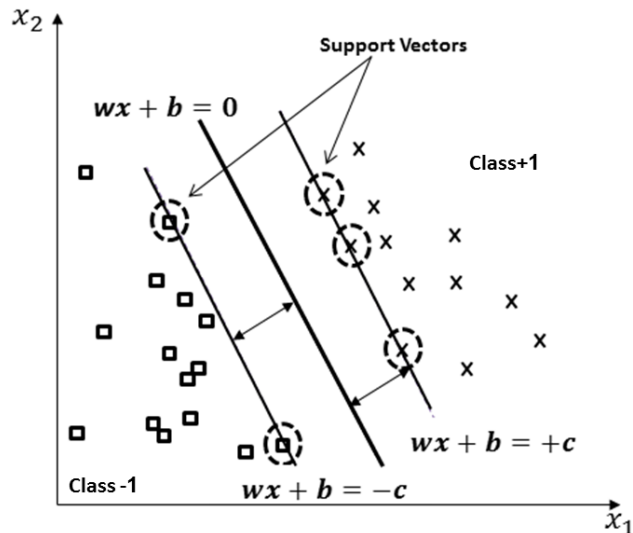


Figure 2) The SVM method to classify the two classes using a linear kernel in two dimensions (Goodarzi Mehr *et al.*, 2012).

In the above equations, T represents transposed matrix, G gamma parameter, d represents the degree of Polynomial kernel and x_j and x_i represent the vector components j and i. In this study, classification of lithological units was

conducted using the above –mentioned three kernels and the degree of polynomial and different gamma values. Afterwards, the results were analyzed. Obviously, in nonlinear SVM kernels, gamma parameters control the form of decision border. Its low values make the decision border linear in form and with increasing its values, the flexibility of decision border increases and therefore the decision border closes further to the form of data cloud of each class. Changes in d parameter increase the flexibility of the separating hyperplane. (Goodarzi Mehr *et al.*, 2012).

3–Sampling method and laboratory studies

According to the field studies undertaken by authors as well as the geochemical, mineralogical, geothermobarometric and geochronologic studies (Fotoohi Rad 1996, 2004 and 2009), Fotoohi Rad *et al.*, (2005), Brocker *et al.*, (2011), Theunssen *et al.*, (2011) and Brocker *et al.*, (2013) the rock units of the studied area are classified into five general groups. Also in several field checking studies, all rock units were sampled. Accordingly, the igneous rocks may be divided into two general groups (1) units related to ophiolite mélangé and (2) Oligo-Miocene volcanic complex.

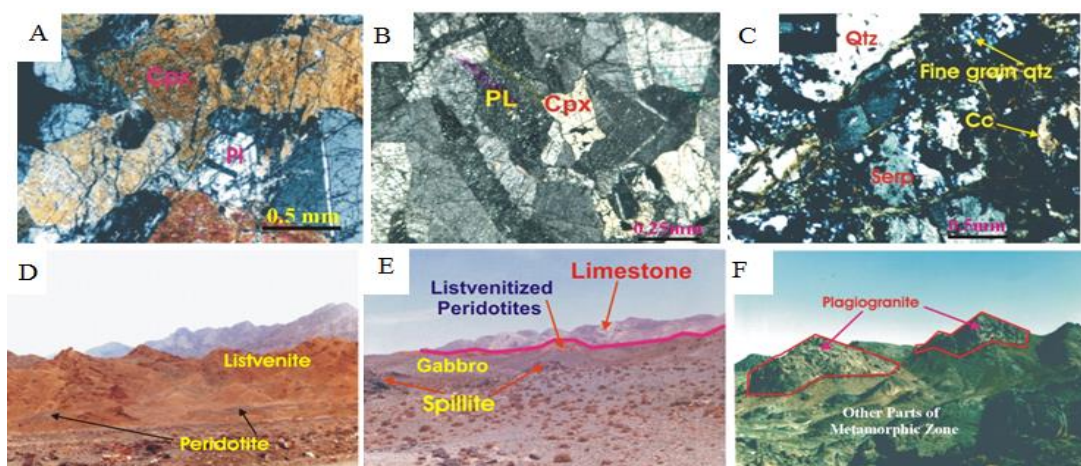


Figure 1) A- sub ophitic to granular texture on isotropic gabbro (XPL). B- Abundant plagioclase Plagiogranite belonging to the ophiolite complex (XPL). C- Microscopic images of silica Listwanite (XPL). D- Listwanitization of peridotites (View of the West). E- Isotropic gabbro and listwanitization peridotite and sequence of Paleocene - Eocene limestones on them (view to north). F- White Plagiogranite cropped (away) and peridotite and the metamorphic zone border (near) (see the West).

3.1–Ophiolite mélange

This unit is composed of (1) magmatogenic units of ophiolitic sequence such as peridotites, gabbro, microgabbros, diabases and plagiogranites and (2) secondary units created from metamorphism and alteration of magmatogenic units, which include metaperidotites, metagabbros, serpentines, milonitized metaplagiogranites and listvinites. The main characteristics of these units are presented in Fig. 3 depicts some microscopic and field image of them.

3.2–Oligo-Miocene volcanics

These volcanics lie in the form of a magmatic arc in the east of the studied area and follow the general trend of the region (Fotoohi Rad, 2004). According to the Tirrol *et al* (1983),

crystallization of these rocks, which also lie in Nehbandan quadrangle map, is younger than igneous rocks comprising ophiolite mélange and belong to volcanic activities in upper Cretaceous, Oligo- Miocene and Quaternary times in eastern Iran. They also include andesite to andesitic basalts of Oligo- Miocene time. In accordance with pyroclastics, andesites, porphyritic andesites and andesitic basalts are usually observed as large outcrops and comprise high mountains. In porphyritic andesite plagioclases, hornblendes, and biotites are observed as coarse crystals and phenocrysts in a ground mass composed of plagioclase microlites and small crystals of amphiboles and opaque minerals. In the samples, plagioclases are altered into serisite and carbonate and to a lesser amount into kaolinite and epidote. Their texture is almost porphyritic. It is worth mentioning that one of the main differences between these rocks with andesitic basalts is the lack of olivine and clinopyroxene in them (Fig. 4).



Figure 4) Microscopic images of rock samples: A - andesite - amphibole of the opacities, B-diorite porphyry, C-andesite basalt - the presence of olivine and pyroxene as phenocrysts in the background of Plagioclase microlite XPL.

3.3–Metamorphic units

Although outcrops of metamorphic rocks are observed in all parts of the studied area, but the majority lie in the metamorphic rocks at the east of ophiolite mélange. Scattered outcrops are observed in other parts of the ophiolite unit. In this metamorphic zone, flyshes and the rocks related to ophiolitic complex, which predominantly have been mafic and ultramafic, are metamorphosed. The main facieses include green schist (including talk schist) facies, epidot- amphibolite schist (including epidote amphibolites and epidote- amphibolite- schist) facies, amphibolite facies (including

amphibolites and garnet-amphibolite schists) (Fig 5).

3.4–Sedimentary units

Although, in comparison with igneous and metamorphic rocks, the sedimentary rocks are less common and diverse but, however, there are several scattered units of this kind in the studied area which include (1) Paleocene - Eocene limestones which outcrop in the eastern part a the area, (2) micritic and sapary limestone, cherts and radiolarites intermingled with ophiolite mélange and flyshes composed of

siltstones, fine sandstones and cherty shales which are predominantly metamorphosed.

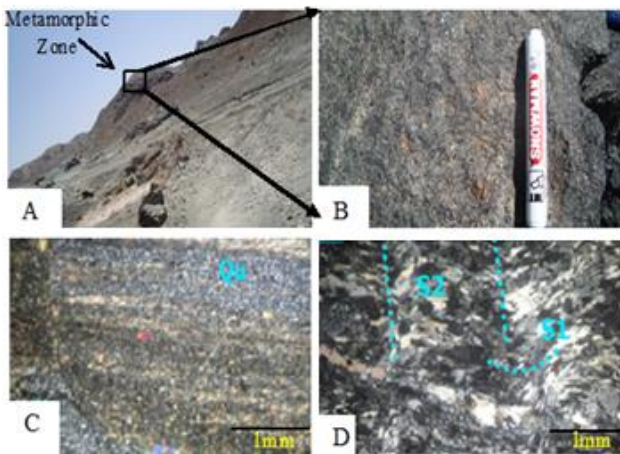


Figure 5) A: the remarkable extent of metamorphic units (see the North East), B: sight near the amphibolite schist with copper mineralization, C: schistosity in rocks → greenschist (XPL); D: schistosity in schist, amphibolite rocks; (XPL).

4–Discussion

4.1–Data analysis

Algorithm analysis in processing of hyperspectral data by Kruse *et al.*, (2003) Leverington (2008), Bahram Beigi *et al.*, (2012) attest to the higher efficiency of processing which are based on spectral pattern in comparison with those which are based on statistical models.

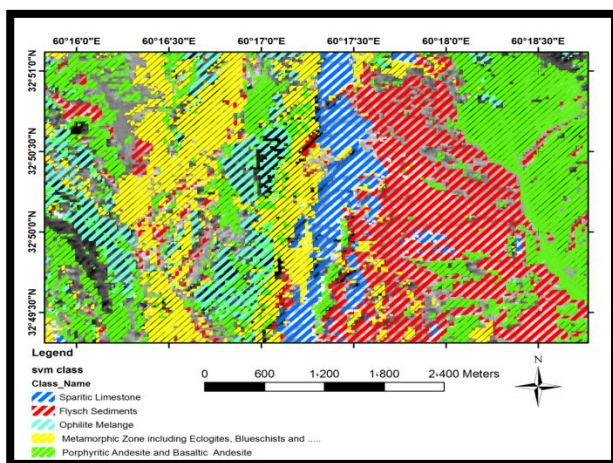


Figure 6) Hyperion image processing area on the output map of SVM method.

Therefore, in order to determine the potential of hyperspectral data to separate ophiolite

mélanges, the SVM algorithm was selected and small areas in five general lithologies were considered for SVM analysis. In this respect, the reflectance pattern of several rock units was used as mixed spectrum of index pixels for training points.

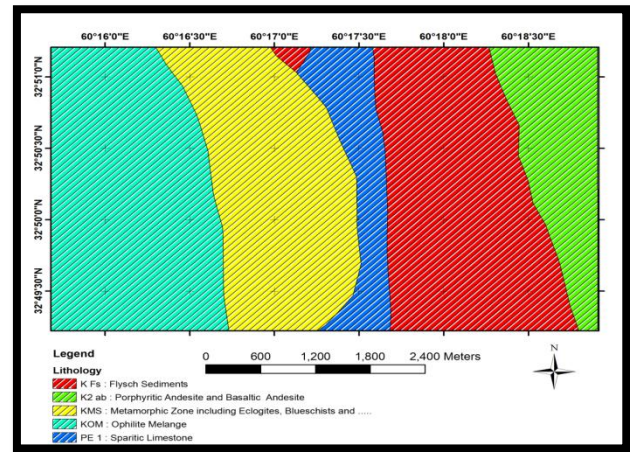


Figure 7) Part of Tabas Messina area map, 1:20000 from Fotoohi Rad (2004).

For every lithological unit, the spectral patterns were determined in images. Eventually, according to theoretic basis of SVM, this processing method is performed on Hyperion data and results were presented as classification image (Fig. 6). Figure 6 shows the extracted classes from processed images of Hyperion image and Figure 7 is part of the map presented by Fotoohi Rad (2004) in the area with 1:20000 scale. Visual comparison of the processed image with geological map of the area represents a favorable conformity in the majority of parts. It is worth mentioning that the geological map is prepared in a very smaller scale and less accuracy, in comparison with the processed images. In the following, the results of hyperspectral processing are compared with field studies.

4.2–Results

In order to access the separation capability of the SVM method on Hyperion image of the area, the enhanced zones were indexed as vector data on Quick bird image of the area and evaluated in field studies. Also for computing

the overall accuracy of the processing method, as indicator of incoherence of rock units in ophiolite mélange, criterion accuracy selected as sampling points. Since band widths in hyperspectral sensors are narrow and very thinner than multispectral one the energy supply of receiving waves by sensor was necessarily taken from wider spaces.

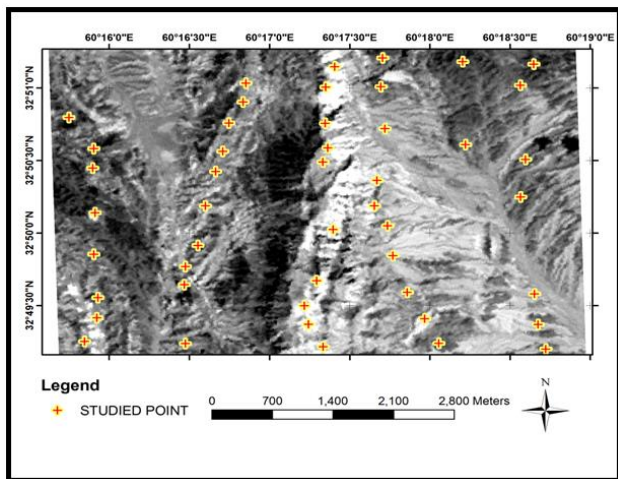


Figure 8) Location of sampling points on the band of 98 in Hyperion image.

As a result, the hyperspectral images lack high spatial resolution (Alavipenah, 2008). In field studies, in order to increase the accuracy and clarity of traverses, vector maps resulting from the processing of Hyperion image were imposed on a Quickbird image having 60-centimeter spatial resolution using GIS technique. These maps which were introduced into a GPS were used as guides to the sites indicated in processing of Hyperion image. Also during field studies, coordinates of the sampling points (Fig. 8) were determined on Hyperion image and the samples were classified into five groups: ophiolite mélange, metamorphic units, Oligocene Miocene volcanic, flyshes and limestones. The coordinates of sampling points were set on Hyperion image as vector data and location of pixels encircling the points indicated as training data on Hyperion image was defined and indexed as the class of each lithology in through image. Controlled classification presents a digital basis for quantitative comparison of the results taken from image

processing and field data in the form of zones limited to pixels having proper values. The Confusion Matrix of indexed pixels in classification and the sampled points in field and laboratory studies (Table 1) were determined by implementing controlled classification methods for pixel data resulted from processing by SVM method on Hyperion image of the studied area.

Table 1) Supervised classification accuracy matrix of the optimal pixels in the SVM image processing method.

Class	Unclassified	An	Calc	Fy	Melang	Meta
Unclassified	7667	4	1	1	4	0
An	2857	3	0	1	1	1
calc	1688	0	8	1	0	0
fy	5125	2	0	5	0	0
Melange	2587	1	0	0	2	1
metamorph	4137	0	1	2	3	8
Total	24061	10	10	10	10	10

The digital basis of comparison in controlled classification method may be expressed by such factors as producer accuracy or user accuracy. In this study, considering the nature of field studies, the best comparison index for using controlled classification matrix is producer accuracy. In the images resulted from processing, of the total classified pixels in each class, 10 pixels were selected and tested in the field, microscopic and laboratory studies. The results are presented as producer accuracy matrix and user accuracy (Table 2).

Table 2) Coefficient of user accuracy and producer accuracy on optimal pixel in the SVM image processing method.

Class	Prod. Acc. (Percent)	User Acc. (Percent)	Prod. Acc. (Pixels)	User Acc. (Pixels)
Unclassified	31.86	99.87	7667/24061	7667/7677
An	30.00	0.10	3/10	3/2862
calc	80.00	0.47	8/10	8/1697
Fy	50.00	0.10	5/10	5/5132
Melange	20.00	0.08	2/10	2/2592
metamorph	80.00	0.19	8/10	8/4151

The producer accuracy of each class is shown in blue color in the Table 2. In these tables "An" refer to Andesitic lava; Calc refer to limestone; Fy refer to Flyshe and Mela refer to mélange.

Among the items affecting the accuracy index we can mention to the degree of polynomial kernel and the gamma value. In the present study, we tested the range values of 0 to 10 and best results obtained in the range of 3 to 7 value with little change so we used the six values for our calculation. Similarly, we test the polynomial kernels of 1 to 6 and the result was that the best overall accuracy is obtained at polynomial kernel value of three so we used only the results in this polynomial kernel value for our judgment. Since our study presents for finding acceptable accuracy rate for ophiolite mélanges area as extremely cluttered lithology units, we have presented only best resulted rates of gamma and polynomial kernel values. Different lithologies in the ophiolite complexes of study area have different accuracy level. Examination of the values expressed in producer accuracy table seems promising, thus the metamorphics and limestones, which contain more separable spectral patterns from each other, have the higher user accuracies because 80 pixels of these lithologies are classified correctly. The lowest user accuracies belong to the completely intermingled part of ophiolite mélange in which only about 20 pixels of these lithologies are classified correctly. Generally, the overall accuracy for all five lithological units is 52%, which considered as a permissible value for separation of extremely sophisticated ophiolite mélanges.

5–Conclusions

In this study, it was shown that hyperspectral data processing could be cheap and useful tools for separating lithological units of ophiolite complexes. Since ophiolite mélanges are one of the most cluttered, highly diverse among geological sitting, their mapping has always been difficult, expensive and time- taking. We tried to present a processing method for simplifying the hard effort for obtaining a good overall accuracy of 52% for it without any extensive field studies. The results of our

studies are such expectations, so that units with minimum contortions such as limestone and metamorphic units have best correlations with field studies than others with high mixing such as mélanges. In the SVM processing method as a good classification scheme for lithology separation, we obtained the best results with the gamma values of six and polynomial kernel value of three.

Acknowledgments:

The authors would like to thank Dr. G. Mountrakis and Dr. S. M. Mortazavi for their kind and careful comments that made the manuscript improved.

References:

- Abedi, M., Norouzi, G. H., Bahroudi, A. 2011. Support vector machine for multi-classification of mineral prospectivity areas. *Computers and Geosciences*: 46, 272–283.
- Alavipanah, S. K. 1382. Application of remote sensing in geology sciences. Institute of Tehran University Publications and Printing; 243 p.
- Alavipanah. S. K. 1388. Modern Remote sensing principles and interpretation of satellite and aerial photos. Institute of Tehran University Publications and Printing; 385p.
- Arvin, M., Robinson, P. T. 1994. The petrogenesis and tectonic setting of lavas from the Baftophiolitic mélange, southwest of Kerman, Iran. *Canadian Journal of Earth Sciences*: 31, 824–834.
- Beiranvand Pour. A., Hashim. M. 2011. The Earth Observing-1 (EO-1) satellite data for geological mapping, southeastern segment of the Central Iranian Volcanic Belt, Iran. *International Journal of the Physical Sciences*: 6, 7638–7650.
- Bindschadler, R., Choi, H. 2003. Characterizing and Correcting Hyperion Detectors Using Ice-Sheet Images. *IEEE Transactions on Geoscience and Remote Sensing*: 41, 1189–1193.
- Brocker, M., Fotoohi Rad, G. R., Thunissen, S. 2011. New time constraints for HP metamorphism and exhumation of mélange rocks from the Sistan suture zone, eastern Iran. An abstract paper in Turkey

- Symposium: Tectonic Crossroads: Evolving Orogens of Eurasia–Africa–Arabia.
- Bröcker, M., Fotoohi Rad, G. R., Burgess, R., Theunissen, S., Paderin, I., Rodionov, N., Salimi, Z. 2013. New age constraints for the geodynamic evolution of the Sistan Suture Zone, eastern Iran. *Lithos*, 170–171, 17–34.
- Bucher, K., Frey, M. 1994. *Petrogenesis of Metamorphic Rocks*. 6th edition. Springer-Verlag Berlin Heidelberg. Printed in Germany, 318p.
- Clark, R. N., Gallagher, A. J., Swayze, G. A. 1990. Material Absorption Band Depth Mapping of Imaging Spectrometer Data Using a Complete Band Shape Least-Squares Fit with Library Reference Spectra, Proceedings of the Second Airborne Visible/Infrared Imaging Spectrometer (AVIRIS) Workshop. JPL Publication: 90–54, 176–186.
- Clark, R. N., Swayze, G. A. 1995. Automated spectral analysis: mapping minerals, amorphous minerals, environmental materials, vegetation, water, ice and snow, and other materials: the USGS tricorder algorithm (abstract). *Lunar and Planetary Science*: 26, 255–256.
- Clark, R. N., Swayze, G. A., Gallagher, A. J., King, T. V. V., Calvin, W. M. 1993. The US Geological Survey, Digital Spectral Library: Version 1: 0.2 to 3.0 microns, U.S. Geological Survey Open File Report: 93–592, 1340 p.
- Coops, N. C., Smith .M. L., Martin, M. E., Ollinger, S. V., Held .A. A. 2002. Predicting Eucalypt biochemistry from HYPERION and HYMAP imagery. In: Proc. IGARSS, Toronto, ON, Canada.
- Crowley, J. K., Clark, R. N. 1992. Aviris study of Death Valley evaporate deposits using least squares band-fitting methods. – JPL Publication: 92–14, 29–31.
- Datt, B., McVicar, T. R., Van Niel, T. G., Jupp, D. L. B., Pearlman, J. S. 2003. Preprocessing EO-1 Hyperion Hyperspectral Data to Support the Application of Agricultural Indexes. *IEEE Transactions on Geoscience and Remote Sensing*: 41, 1246–1259.
- Felde, G. W., Anderson, G. P., Adler-Golden, S. M., Matthew, N. W., Berk, A. 2003. Analysis of Hyperion data with the FLAASH atmospheric correction algorithm. Proceedings of the International Geoscience and Remote Sensing Symposium (IGARSS). Toulouse, 21–25 July 2003, 90–92.
- Fotoohi Rad, G. R. 1996. A study of petrology, petrography and geochemistry of ophiolite mélange of north west of Drah region (southeast of Birjand) with a view on the region's economic potential. Master Thesis, Department of Geology, Tarbiat Moallem University, Tehran, 230p.
- Fotoohi Rad, G. R. 2004. Petrology and geochemistry of metamorphosed ophiolitic of East of Birjand. Education Ph.D. dissertation, Department of Geology, Tarbiat Moallem University, Tehran. 323p.
- Fotoohi Rad, G. R., Droop, G. T. R., Burgess, R. 2009. Early cretaceous exhumation of High-Pressure Metamorphic rocks of the Sistan Suture Zone, eastern Iran. *Geological Journal*: 44, 104–116.
- Genderen, V. J. L., Lock, B. F. 1978. Remote sensing: statistical testing of thematic map accuracy. *Remote Sensing of Environment*: 7, 3–14.
- Geological Survey of Iran. 1972. Geological map of Shahr-e-babak; 1:100000.
- Gersman, R., Ben-Dor, E., Beyth, M., Avigad, D., Abraha, M., Kibreab, A. 2008. Mapping of hydrothermally altered rocks by the EO-1 Hyperion sensor, northern Danakil Depression, Eritrea. *International Journal of Remote Sensing*: 29, 3911–3936.
- Ghazi, A. M., Hassanipak, A. A., Mahone, J. J., Duncan, R. A. 2004. Geochemical characteristics, $^{40}\text{Ar}/^{39}\text{Ar}$ ages and original tectonic setting of the Band-e Zeyar-at Anarophilite, Makranaccretionary prism, S.E. Iran. *Tectonophysics*: 393, 175–196.
- Gilbert, J. M., Park, J. R. C. F. 1997. *The geology of ore deposits*. Freeman and Company, New York. 985p.
- Gomes-Pugnair, M. T., Azor, A. Fernandez-Soler, J. M., Lopez Sanchez-Vizcaino, V. 2003. The amphibolite from the Ossena-Morena /Central Iberian Variscan suture (Southwestern Iberian Massif): geochemistry and tectonic interpretation. *Lithos*: 68, 23–42.
- Goodarzi Mehr, S., Abbaspour, R. A., Ahadnejad, V., Khakbaz, S. B. 2012. Compared to the maximum likelihood

- method, support vector machine and neural network methods for the separation of lithological units. *Iranian Journal of Geology*: 6, 75–92
- Goodenough, D. G., Dyk, A., Niemann, K. O., Pearlman, J. S., Hao, Ch., Han, T., Murdoch, M., West, C. 2003. Processing Hyperion and ALI for forest classification, *IEEE Transactions on Geoscience and Remote Sensing*: 41, 1321–1331.
- Gupta, R. P. 2003. *Remote Sensing Geology*, 2nd ed., Springer, Berlin, 654p.
- Honarmand, M., Ranjbar, H., Shahabpour, J. 2012. Application of Spectral Analysis in Mapping Hydrothermal Alteration of the Northwestern Part of the Kerman Cenozoic Magmatic Arc, Iran. *Journal of Sciences, Islamic Republic of Iran*: 22, 221–238.
- Hubbard, B. E., Crowley, J. K., Zimelman, D. R. 2003. Comparative alteration mineral mapping using visible to shortwave infrared (0.4–2.4 μ m) Hyperion, ALI, and ASTER imagery, *IEEE Trans. Geosci. Remote Sensing*: 41, 1401–1410.
- Khurshid, K. S., Staenz, K., Sun, L., Neville, R., White, H. P., Bannari, A., Champagne, C. M., Hitchcock, R. 2006. Preprocessing of EO-1 Hyperion data. *Canadian Journal of Remote Sensing*: 32, 84–97.
- Kovacevic, M., Bajat, B. Trivic, B., Pavlovic, R. 2009. Geological Units Classification of Multispectral Images by Using Support Vector Machines. *Intelligent Networking and Collaborative Systems*, 2009. *INCOS International Conference*: 267–272.
- Kruse, F. A. 2003. Preliminary Results – Hyperspectral mapping of coral reef systems using EO-1 Hyperion, Buck Island, U.S. Virgin Islands: In proceedings 12th JPL Airborne Geoscience Workshop, Jet Propulsion Laboratory. Publication 04-6 (CD-ROM), p. 157–173.
- Kruse, F. A., Boardman, J. W., Huntington, J. F. 2002. Comparison of EO-1 Hyperion and Airborne Hyperspectral Remote Sensing Data for Geologic Applications: in Proceedings, SPIE Aerospace Conference, 9–16 March 2002, Big Sky, Montana.
- Kruse, F. A., Boardman, J. W., Huntington, J. F. 2003. Comparison of Airborne Hyperspectral Data and EO-1 Hyperion for Mineral Mapping. *IEEE Transactions on Geoscience and Remote Sensing*: 41, 1388–1400
- Kruse, F. A., Boardman, J. W., Huntington, J. F. 2003. Comparison of airborne hyperspectral data and EO-1 Hyperion for mineral mapping. *IEEE Transactions of Geosciences and Remote Sensing*: 41, 1388–1400.
- Kruse, F. A., Lefkoff, A. B., Boardman, J. B., Heidebrecht, K. B., Shapiro, A. T., Barloon, P. J., and Goetz, A. F. H. 1993. The Spectral Image Processing System (SIPS) - Interactive Visualization and Analysis of Imaging Spectrometer Data. *Remote Sensing of Environment: Special issue on AVIRIS*, 44, 145–163.
- Leverington, D. W. 2008. Discrimination of geological end members using Hyperion imagery: Preliminary results, Big Bend National Park, Texas. *IEEE International Geosciences and Remote Sensing Symposium*, Boston, Massachusetts.
- Moghadam, H., Stern, R. J., Chiaradia, M., Rahgoshay, M. 2013. Geochemistry and tectonic evolution of the Late Cretaceous Gogher–Baftophiolite, central Iran. *Lithos*, 168–169, 33–47.
- Mountrakis, G., Im, J., Ogole, C. 2011. Support vector machines in remote sensing: A review. *ISPRS Journal of Photogrammetry and Remote Sensing*: 13, 247–259.
- Online space diploma of iran; www.isa.ir.
- Pearlman, J. S., Barry, P. S., Segal, C. C., Shepanski, J., Beiso, D., Carman, S. L. 2003. Hyperion, a Space Borne Imaging Spectrometer. *IEEE Transactions on Geosciences and Remote Sensing*: 41, 1160–1173.
- Ramsey, E., Rangoonwala A., Nelson .G, Ehrlich, R., Martella, K. 2004. Generation and validation of characteristic spectra from EO-1 Hyperion image data for detecting the occurrence of the invasive species, Chinese tallow. *International Journal of Remote Sensing*: 26, 1611–1636.
- Remote Sensing Tutorial of NASA; www.rst.gsfc.nasa.gov.
- Robb, L. 2005. *Introduction to Ore Formation Processes*; Blackwell Publishing Company, UK, 373p.
- San, B. T., Suzen, M. L. 2010. Evaluation of different atmospheric correction algorithms for EO-1 Hyperion imagery; *International*

- Archives of the Photogrammetry. Remote Sensing and Spatial Information Science: 38, 392–398.
- Sarup, J. 2011. Comparison of QUAC and FLAASH Atmospheric Correction Modules on EO-1 Hyperion Data of Sanchi. International Journal of Advanced Engineering Sciences and Technologies: 4, 178–186.
- Staenz, K., Neville, R. A., Clavette, S., Landry, R., White, H. P. 2002. Retrieval of Surface Reflectance from Hyperion Radiance Data. IEEE Geoscience and remote sensing letters: 1, 1419-1421.
- Tirrul, R., Bell, I. R., Griffis, R. J., Camp, V. E. 1983. The Sistan Suture Zone of eastern Iran. Geological Society of America Bulletin: 94, 134–150.
- USGS. 2004. Earth Observing 1, downloaded on May, 2009, from, Url: <http://eol.usgs.gov/>.
- Weber Diefenbach, K., Davoudzadeh, M., Alavi-Tehrani, N., Linsch, G. 1984. Paleozoic ophiolites in Iran: Geology and geochemistry, and geodynamic implication. Ofioliti: 11, 305–383.
- Website of Geological Organization and Mineral Exploration of Iran; Url: www.gsi.ir.
- Yuanjin, X., Hongchao, M., Shiyu, P. 2014. Study on identification of altered rock in hyperspectral imagery using spectrum of field object. Ore Geology Reviews: 56, 584–595.